CHARACTERIZATION OF FISH-BONE TYPE RC WALL BUILDINGS THROUGH ANALYTICAL FRAGILITY FUNCTIONS

M.J. Echeverría[(1)], R. Jünemann[(2,3)]

[(1)] *PhD Candidate, Department of Structural and Geotechnical Engineering, Pontificia Universidad Católica de Chile,* moecheverria@uc.cl
[(2)] Assistant Professor, *Department of Structural and Geotechnical Engineering, Pontificia Universidad Católica de Chie,* rjunemann@ing.puc.cl
[(3)] *Researcher, National Research Center for Integrated Natural Disaster Management (CIGIDEN), CONICYT/FONDAP/15110017,* rjunemann@ing.puc.cl

Abstract

The seismic behavior of reinforced concrete (RC) buildings during the last decade has been successful in terms of preventing the overall or partial collapse and protecting human life. However, high-intensity earthquakes have produced significant damage to this kind of structures. For example, after the 2010 Chile earthquake, extensively localized brittle damage was observed in RC wall buildings. This rupture mechanism was characterized by concrete crushing and buckling of the vertical reinforcement. Most of the damage occurred in the lower stories of medium-rise buildings constructed after the year 2000 and was due in part to the use of thin unconfined RC walls subjected to high axial load ratios. Although significant damage was observed in only approximately 2% of the stock of RC wall buildings taller than nine stories, there are many other buildings with almost identical structural characteristics to the damaged ones that presented minor damage, or that did not present damage at all. Therefore, it is necessary to understand and quantify the vulnerability of this large number of buildings that may be prone to suffer the same type of brittle failure by future seismic events.

This research is focused on medium-rise RC wall buildings with floor plans commonly used for residential buildings in Chile and other seismic countries. These buildings have a plan configuration that resembles that of a "fish-bone" structure, with long corridor walls in the longitudinal direction and perpendicular walls in the transverse direction. Although this typology is widely used in seismic regions around the world, its characterization through analytical or empirical fragility and vulnerability functions is poor. Available characterizations are based mainly on over-simplified models that cannot accurately represent the complex 3D behavior of this type of buildings. Thus, this research aims to develop analytical fragility functions based on simplified but accurate models validated with sophisticated 3D inelastic finite element models of a real building.

Analytical fragility functions are built from inelastic finite element models of representative building slices modeled using the software DIANA. Two different building conditions are analyzed in this study. First, the typical Chilean buildings constructed between 2000 and 2010 are considered, characterized by thin unconfined RC walls. Second, confined RC wall buildings are evaluated, which represent the new constructions built after the changes in Chilean seismic code in 2011, are evaluated. Incremental dynamic analysis is performed with the use of a series of ground motion records from the 2010 Chile earthquake. Engineering demand parameters are calculated and related to damage measures, in order to obtain fragility functions, considering various damage states: slight, moderate, extensive, and complete. The results of this research could be used to develop a robust analytical framework for vulnerability assessment of RC wall buildings constructed before and after the 2010 earthquake and evaluate the effects of the changes in Chilean seismic code.

Keywords: reinforced concrete wall buildings; fragility curves; earthquake vulnerability; nonlinear dynamic analysis

1. Introduction

Reinforced concrete wall buildings are commonly used in seismic countries such as Chile and New Zealand, among others [1, 2], as an effective force resisting system for seismic and gravitational loads. In most countries, seismic codes for buildings are based on traditional design philosophy, which aims to prevent collapse and to preserve life in high-intensity earthquakes but does not limit the damage to repairable levels. Consequently, this philosophy leaves RC walls vulnerable to suffer severe damage during strong seismic excitations [3]. This damage was observed following many recent earthquakes, including the Mw 8.8, 2010 Chile earthquake. Although the performance of Chilean buildings was satisfactory according to available codes, significant economic losses occurred, associated with direct and indirect costs related to seismic damage. Approximately 2% of 2000 RC buildings taller than 9 stories suffered moderate to severe damage during the earthquake [4, 5]. The damage was evidenced mostly in modern buildings constructed after the year 2000, with a high wall density, but generally with thin unconfined RC walls subjected to high axial stress due to gravitational loads, which in turn increase due to dynamic effects [6].

In Chile, approximately 78% of the RC building stock are shear wall buildings [7] typically intended for residential use, and with a “fish-bone” type floor plan configuration. This typical plan has a central longitudinal corridor with RC walls and transverse walls, as shown in Fig.1a. Although a vast majority of medium-rise RC wall buildings showed an adequate seismic performance during the 2010 Chile earthquake, a repetitive brittle failure was observed, as illustrated in Fig.1b and Fig.1c. This rupture mechanism was characterized by concrete crushing and buckling of the vertical reinforcement in a zone that extends from the wall boundary well into the web of the wall, typically observed in the lower building stories [4, 5]. Despite “fish-bone” RC buildings are extensively used, the characterization of this type of buildings through analytical or empirical fragility functions is poor. Therefore, this paper focuses on the fragility analysis of this typology. A real RC wall building damaged during the 2010 Chile earthquake is considered as a case-study building, and two building conditions are evaluated. First, the building is modeled considering its original condition, i.e., thin unconfined walls, which represents a large amount of RC wall buildings constructed before the year 2010. Second, the building is evaluated considering its repaired condition, i.e., thicker and confined walls, which represents not only the buildings repaired, but also the new buildings constructed after the changes in Chilean seismic design provisions in 2011. The fragility functions are developed through incremental dynamic analyses (IDA) [8] using simplified 3D inelastic finite element models (FEM) and a set of 14 ground motion recorded during the 2010 Chile earthquake. The inter-story drift of the first story is considered as an engineering demand parameter (EDP) and related to specific damage measure (DM). Four damage states proposed in HAZUS-HM technical manual [9] for RC walls are used.

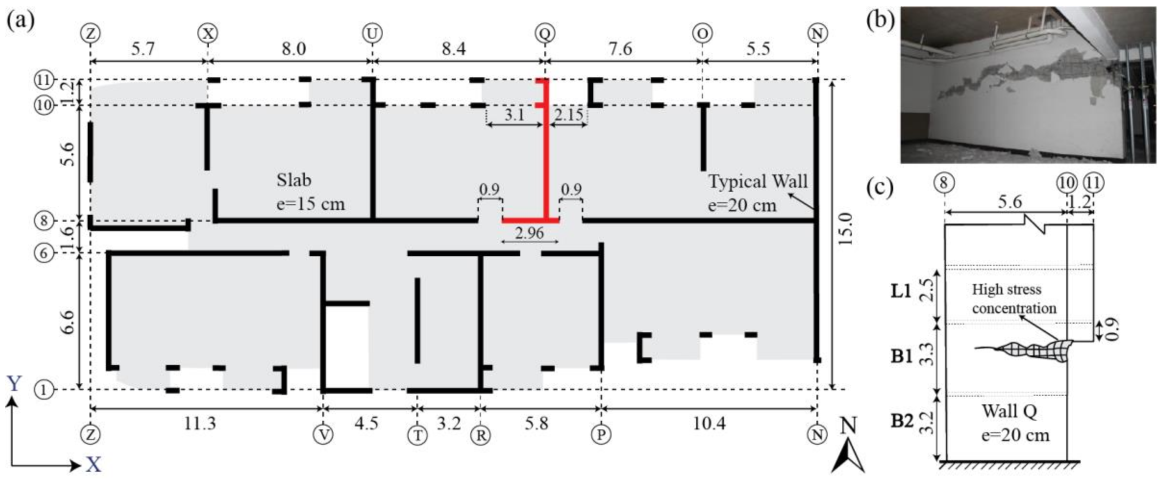

Fig. 1 – Typical “fish-bone” RC building: (a) floor plan layout (dimensions in meters); (b) typical failure observed after 2010 Chile earthquake (damage information provided by Sopoerer & Asociados); (c) elevation of wall Q with typical flag-shape

2. Building description

The RC wall building selected as a case-study is located in Santiago, Chile. It is a residential building with 18 stories and two basements, with a typical "fish-bone" floor plan configuration, as indicated the Fig.1a. The building typically has 15 cm thick slabs and 20 cm thick walls. This building represents the typical Chilean residential building constructed before the 2010 earthquake, with thin and unconfined walls. The selected building suffered severe damage in some walls during the Maule 2010 earthquake, like other RC wall buildings located in Santiago, Viña del Mar, and Concepción [4, 5]. The most severe damage was observed in the transverse RC walls of the north side of the building, particularly in the axis Q, U, and N (Fig.1a). These walls have a flag-shape configuration with an irregularity in the transition between the basements and the first story (Fig.1c). The damage was concentrated just below the irregularity, as shown in Fig.1b and Fig.1c, for wall Q.

Recent studies have developed sophisticated 3D inelastic models of the case-study building [10]. These models consider inelastic behavior concentrated in the vertical elements of the first story and basements, while the rest of the building remains with linear-elastic behavior. The models can replicate the brittle failure observed after the earthquake. However, these are full 3D building models with a high computational cost, especially when thinking in IDA [8], which requires analyzing the response of one building to multiple seismic records. Therefore, it is necessary to develop a simplified model able to accurately reproduce the response of the complex 3D model at a lower computational cost.

3. Inelastic finite element model

Since IDA is a computationally demanding method involving a series of nonlinear time-history analysis, a simplified model is proposed in this section, which is a 3D nonlinear FEM of a building slice. The proposed model allows for performing IDA within reasonable computational time while capturing the nonlinear structural behavior reliably.

3.1 Model description

Nonlinear finite element models of RC walls are developed using the software DIANA [11] since it has shown good results in previous research [6, 10]. Concrete was modeled using the Q20SH element, which is a curved shell quadrilateral element with four nodes and four Gauss-point quadrature [11]. Reinforcement was modeled using the BAR element, which is an embedded element and follows the assumption of perfect bonding [11]. The total strain rotating crack approach was used to model concrete behavior, in which the principal stress tensor is evaluated in the principal strain directions. DIANA presents different alternatives to simulate the inelastic behavior in tension and compression based on predefined constitutive models. The parabolic model was considered for compressive behavior, while the Hordijk model was used for tensile behavior. The compressive fracture energy for the parabolic model G_c was obtained from recommendations given by Nakamura and Higai [12]. The Mode-I fracture energy G_f for the Hordijk model was selected based on the CEB-FIP code recommendations. The behavior of reinforcing steel was modeled using the Menegotto-Pinto model.

3.2 Model validation

Two RC specimens tested on an experimental campaign by Dazio et al. [13], are modeled using the material definitions described in the previous section aimed to validate the proposed finite element models. The first specimen WSH4 corresponds to an unconfined rectangular wall with an axial load ratio (ALR) of 5.7%. The second specimen WSH3 corresponds to another rectangular wall but with confining reinforcement at both ends with ALR of 5.8%. Fig.2a shows the geometry of the selected specimens, Fig.2b and Fig.2c show the corresponding cross-sections of each specimen. Material properties obtained from existing tests were considered when they were available; otherwise, recommendations proposed in the previous section were used. Furthermore, the parameters for the Menegotto-Pinto model were considered in the range of values suggested by Papadrakakis et al. [14].

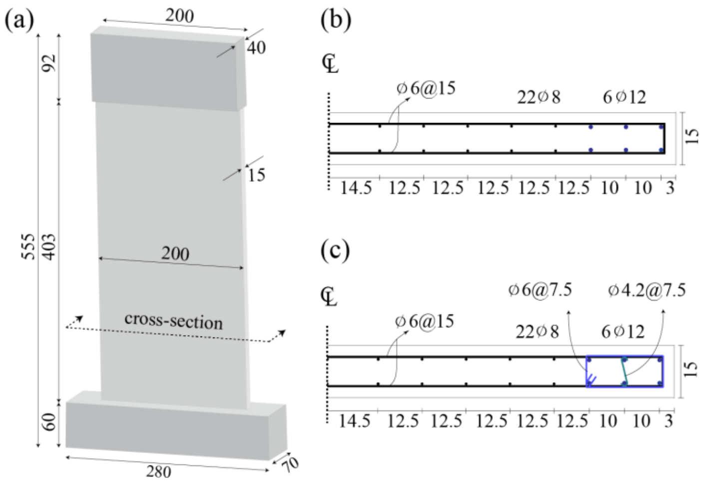

Fig. 2 – Geometry of selected specimens: (a) Dimensions in centimeters; (b) cross-section specimen WSH4; (c) cross-section specimen WSH3

3.2.1 Unconfined specimen

Specimen WSH4 was modeled first since it represents an unconfined thin shear wall similar to those constructed before the 2010 Chile earthquake and to those found in the case-study building. In this case, concrete strength f_c' and Young's modulus E_c were obtained from cylinder specimens [13]. The confinement ratio calculated for this specimen, according to Mander, Priestley and Park [15] was K=1.01, which was very low, and hence, only unconfined concrete was considered in the finite element model. For unconfined concrete, the compressive fracture energy G_{uc} proposed by Nakamura and Higai [12] was used. Finally, tensile strength f_t and tensile fracture energy G_t were estimated according to CEB-FIP. Fig.3a shows schematically the finite element model for mesh size h≈35 cm, where the displacements at the base nodes are constrained. An axial load of 695 kN and the same displacement pattern of the experimental tests were applied. The nonlinear analysis was conducted with the Quasi-Newton iterative method. The tolerances used were 10^{-3} for force and 10^{-4} for energy. Fig.3b displays the lateral load versus the top displacement of the specimen. The global load-displacement response predicted by the model is in good agreement with the experimental measurements. Further, the model provides good results for the strength degradation and ultimate behavior of the specimen.

3.2.2 Confined specimen

Specimen WSH3 is a rectangular specimen with the same layout as specimen WSH4 but with confined boundary elements, as shown in Fig.2c. This specimen corresponds to a ductile wall in terms of the reinforcement properties, the longitudinal reinforcement contents, and the detailing, according to Central European standards [13]. It was considered to represent the confined walls, such as those built after the 2010 earthquake, according to current Chilean code requirements for special boundary elements. The confinement ratio calculated according to Mander, Priestley and Park [15] was K=1.10, which is not negligible. Confined concrete was used for boundary elements and unconfined for interior elements in the finite element model. The compressive fracture energy proposed by Nakamura and Higai [12] was considered for unconfined concrete G_{uc}. For confined concrete, the compressive fracture energy G_{cc} was estimated based on an equivalent element of unconfined concrete [6], and Karthic & Mander constitutive models [16]. Tensile strength and tensile fracture energy were estimated as in the previous case, according to CEB-FIP. Fig.3c shows the finite element model for mesh size h≈35 cm. An axial load of 686 kN was applied as a first load case, and lateral displacement is applied gradually as a second load case. The same iterative method and tolerances used in the previous case were considered. Fig.3d compares the numerical predictions with experimental measurements in terms of lateral load versus top displacement. As can be seen, the hysteretic response of the specimen was reasonably well-predicted by the model.

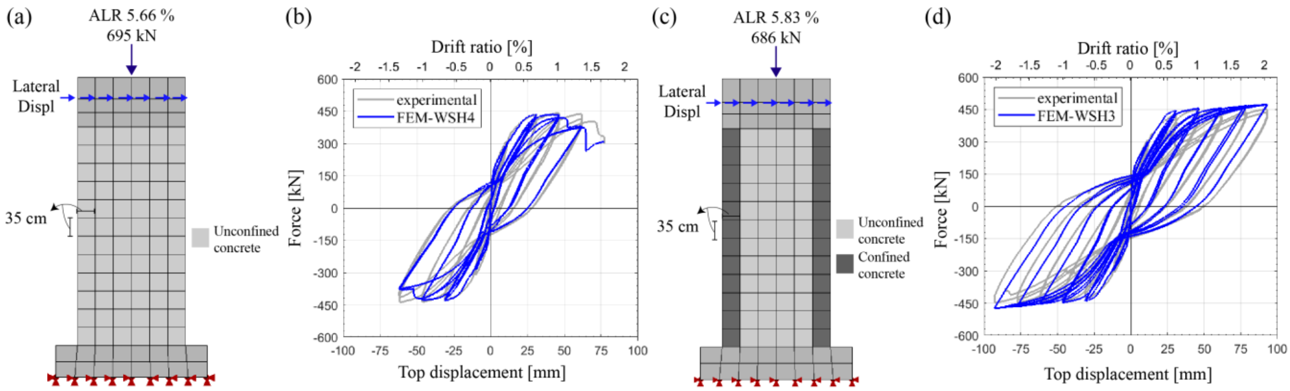

Fig. 3 – Specimens: (a) FEM WSH4 in DIANA; (b) lateral load-top displacement response of WSH4; (c) FEM WSH3 in DIANA; (d) lateral load-top displacement response of WSH3

3.3 Simplified FEM of RC wall building

Earlier studies [10] developed a sophisticated 3D inelastic FEM of the selected building, which was able to predict the observed damage considering a ground motion record located near the building but with a high computational cost. Additionally, studies showed that conventional 2D models of isolated walls could be more efficient in terms of computational cost but are not capable of capturing the expected behavior of the building [6, 10]. This issue occurs because the isolated wall model neglects the interaction between the wall and the rest of the building and is not able to predict the expected increase in the axial load due to the seismic action that was key in the observed damage. Thus, a new simplified model is proposed in this investigation aims to capture these effects and explain the nonlinear behavior within reasonable computational time.

An inelastic FEM of resisting plane Q displayed in Fig.1a was developed in the software DIANA [11], aimed to replicate the damage pattern observed in Fig.1b and Fig.1c. This wall has a flag-shaped configuration with a noticeable irregularity at the ground level, where the wall changes in length and cross-section. Indeed, the wall shortens from 695 cm at the first story to 575 cm at the basement, and the orthogonal wall flanges of 70 cm at the first story are also discontinued at the basement, as shown in Fig.4. The vertical boundary reinforcement increases from 4ϕ22 to 4ϕ25 in the basement; additional ϕ8 stirrups separated at 17 cm are included at the basement. The elevation of wall Q is illustrated in Fig.4a, and the cross-section at the basements and the first story are shown in Fig.4b and Fig.4c, respectively. Since the boundary confinement is limited, only unconfined concrete is considered in the finite element model.

The nominal properties specified in the project were used, f_c'=25 MPa for concrete compressive strength, and yield stress of f_y=420 MPa for steel A630-420H. Following the recommendations discussed in the previous sections, the following properties were considered: compressive energy G_{uc}=44 MPa-mm, tensile fracture energy G_f=0.110 MPa-mm; and tensile strength f_t=2.58 MPa. Elastic modulus of E_c=25600 MPa and E_s=200000 MPa were assumed for concrete and reinforcing steel, respectively. The Menegotto-Pinto model was considered for the steel with the parameters used in section 3.2. Rayleigh damping was assumed for the model. The damping matrix used was C_r=0.4528M+0.0051$K_{elastic}$. These values were calculated imposing 5% of critical damping at the first two vibration modes.

As in the sophisticated 3D FEM developed by Jünemann et al. [10], this model also considered inelastic behavior concentrated in the vertical elements of the first story and two basements. Since no significant damage was reported on other elements of the selected building after the 2010 Chile earthquake, the rest of the structure is modeled with linear elastic behavior, including slabs. Thus, nonlinear concrete and reinforcing steel rebars were considered only in vertical elements until the 1st floor, and from the 2nd floor and up, linear concrete is used, reducing stiffness in accordance with ACI 318-14. A sensitivity analysis was developed considering inelastic behavior on more floors. Results showed that the computational cost significantly increases with the number of floors considered with nonlinear behavior, while the response obtained did not differ significantly from the one obtained in the proposed model.

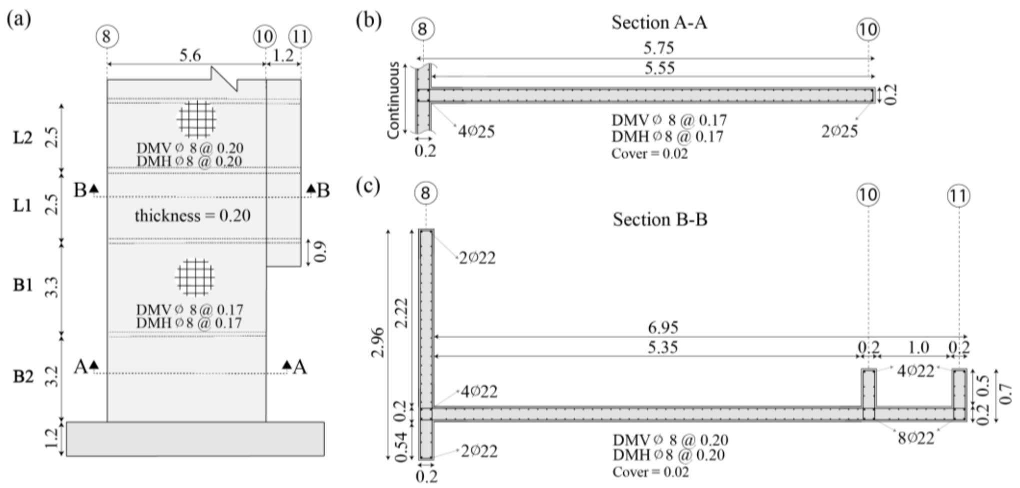

Fig. 4 – Wall at axis Q (dimensions in meters): (a) structural specifications of wall Q; (b) section A-A of axis Q at basements; (c) section B-B of axis Q from first story and above

In order to capture the 3D interaction between the wall Q and the rest of the structure, a complementary portion of the building is required. Since the building is not exactly symmetrical and a real slice of the building is complex as shown in Fig.1a, a fictitious building slice is modeled, where wall Q is replicated as in a mirror, as shown in Fig.5. This model configuration was proposed earlier by Tagle et al. [17], showing good results for static nonlinear analyses. The geometry of the simplified model is shown schematically in Fig.5a, and the cross-section at the basements and the first story are illustrated in Fig.5b and Fig.5c, respectively. The building model was restrained at the base of the second basement. Soil-structure interaction was not accounted for in the model.

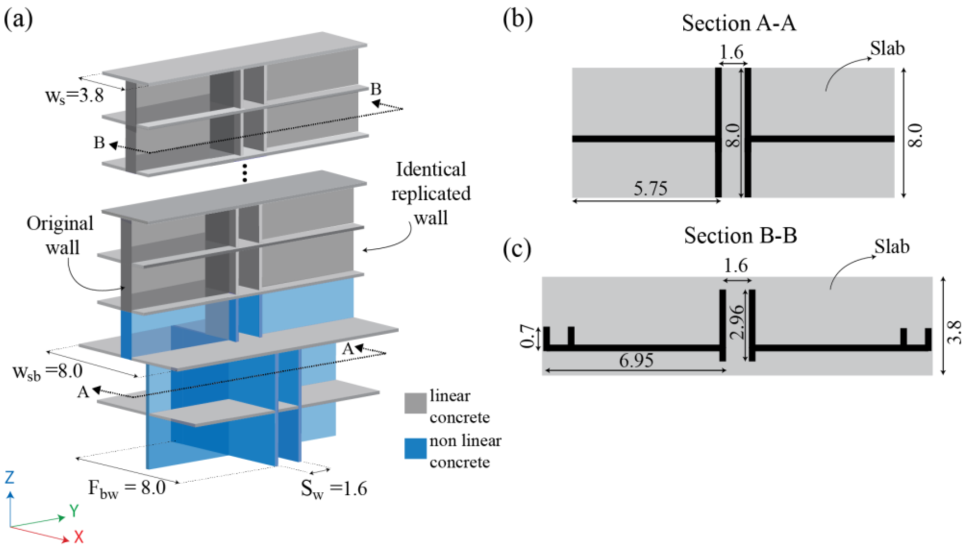

Fig. 5 – Simplified model (dimensions in meters): (a) schematic 3D view of the simplified FEM (adapted from Tagle et al. 2019); (b) section A-A at basements; (c) section B-B from first story and above

3.3.1 Analysis results for building constructed before the 2010 earthquake

The simplified model described in the previous section was performed and results compared with the full 3D nonlinear model of the same building developed earlier [10]. Modal analysis of the simplified model (SFEM-Pre2010) showed that the first mode corresponds predominantly to the translational mode along Y-direction, which has a fundamental period of 1.03 seconds, while the one obtained from the referential model of the entire building (FEM-Building) was 1.1 seconds.

Inelastic dynamic analysis of both models was performed considering the North-South component of the Puente Alto record, applied in the Y-direction (Fig.5a) of the building, which was the direction where most of the damage was concentrated. This ground motion was recorded during the 2010 Chile earthquake in a station near the considered building. Before imposing the lateral load due to earthquake, the gravitational loads D+0.25L were applied as a nodal mass. D and L represent dead and live loads, respectively. These values were obtained from a referential linear elastic model of the building developed in the software ETABS.

Fig.6a shows the lateral roof displacements measured at the center of mass (CM) of the top floor along the Y-direction for both models. Results of the two nonlinear models are in good agreement throughout the response showing peak displacements of 17.2 cm and 13.2 cm for SFEM-Pre2010 and FEM-Building, respectively. This difference is in the range of epistemic uncertainties proposed by Chacón et al. [18]. In both cases, peak displacements occurred at the same time, approximately 60 seconds. Additionally, ALR in the walls is also evaluated since it has shown to be closely related to the observed damage [6]. ARL is calculated as the quotient $P/(A_g f_c')$, where P is the axial load in the wall; A_g is the area of the structural element; f_c' is the characteristic concrete strength. Fig.6b shows results for the critical section ALR. The critical section considered was just below the vertical irregularity shown in Fig.1c. The two inelastic models predict an abrupt brittle failure in the critical RC wall. High ALR causes failure of the walls and loss of their load-carrying capacity at the peak displacement. Three zones can be identified in Fig.6b: i) an essentially linear-elastic zone; ii) a brittle failure, and iii) residual cycles.

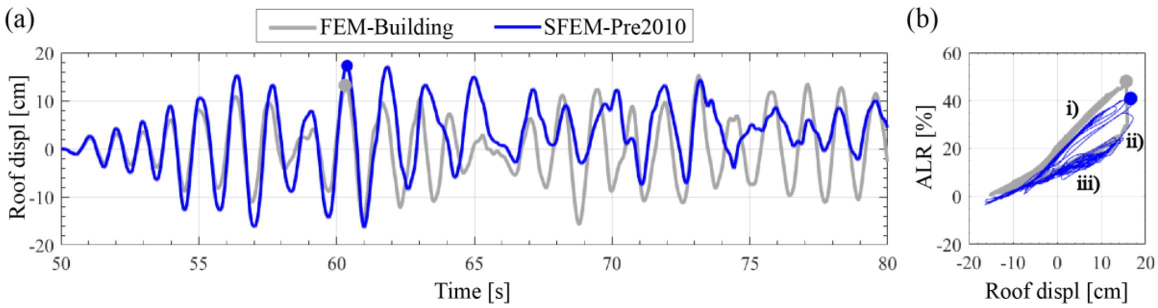

Fig. 6 – Results for the North-South component of the Puente Alto record: (a) lateral roof displacements in the Y-direction at the CM at the roof; (b) ALR at the critical section of wall Q versus lateral roof displacements

3.3.1 Analysis results for building repaired after the 2010 earthquake

The Chilean seismic codes in place before the 2010 earthquake did not limit the axial load and did not establish a minimum thickness for shear walls [19, 20]. Although these codes referred to ACI 318-95 seismic provisions, the requirement of the special boundary elements was excluded due to Chilean buildings behaved well during the 1985 earthquake. However, during the following decade, construction and design practices changed. The buildings tended to be taller and with increasingly thin walls, which led to higher axial stress associated with the non-ductile damage observed after the 2010 earthquake. This seismic event demonstrated the deficiencies of Chilean design codes, and consequently, some provisions were modified, and two new decrees were approved. The first decree N°60 [21] modified the Chilean code for RC design [19], placing a limit of 0.35 f'_c to the maximum compressive stress in walls, defining new criteria for wall confinement and a minimum thickness of 30 cm. The second decree N°61 [22], modified the Chilean code for seismic design of buildings [20], by changing the soil classification and the design spectra.

From the model validated in the previous section, a second building is modeled and evaluated under the same loads. This model corresponds to the building on its repaired condition after the 2010 earthquake, with the reparation technique shown in Fig.7. The building was repaired and strengthened by adding special boundary elements on the transverse walls of the first story and basements. The shear strength was also increased by increasing the wall thickness from 200 mm to 320 mm in the second basement to the 3rd floor [23]. The repaired RC wall building complies with the requirements of current seismic design codes. Therefore, this condition could also represent the modern constructions built after the changes in Chilean code in 2011. Confined concrete was considered in the boundary elements of the finite element model. The confinement ratio calculated according to Mander, Priestley and Park [15] was K=1.5. Properties for unconfined concrete and reinforcing steel were indicated in previous sections. For confined concrete, compressive strength was f_{cc}=30 MPa, and the compressive fracture energy G_{cc}=228 MPa-mm. As in the previous model, Rayleigh damping was assumed.

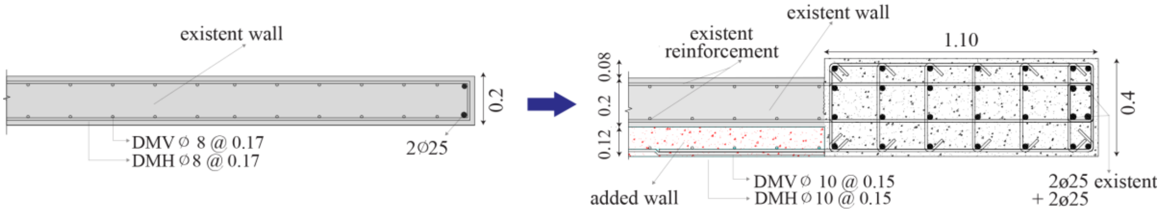

Fig. 7 – Reparation technique (dimensions in meters)

The modal analysis showed that the first mode corresponds predominantly to the translational mode along Y-direction, which has a fundamental period of 0.91 seconds. The lateral roof displacements at the top floor along the Y-direction for the repaired building (SFEM-Post2010) compared with the conventional building presented in the previous section (SFEM-Pre2010) is displayed in Fig.8a. The peak response for the repaired building model is 17.9 cm, slightly higher than the conventional building response, and was presented approximately 10 seconds later. Fig.8b shows ALR versus the roof lateral displacement. Despite the large ALR in compression, neither crushing nor buckling was observed in the walls, and the behavior was essentially elastic.

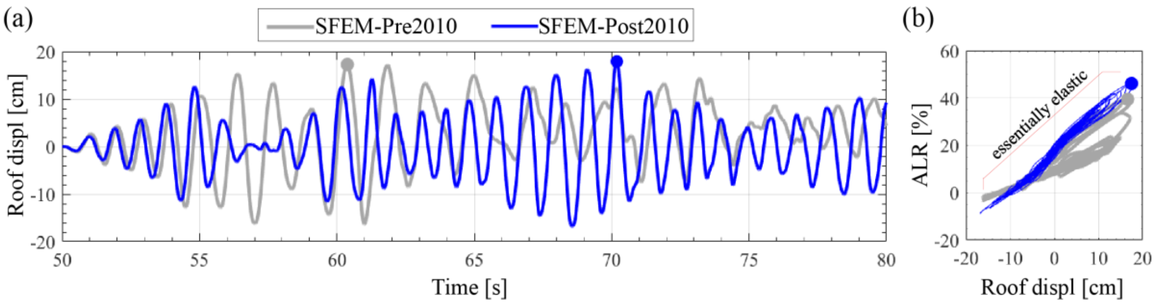

Fig. 8 – Results for the North-South component of the Puente Alto record: (a) lateral roof displacements in the Y-direction at the CM at the roof; (b) ALR at the critical section of wall Q versus lateral roof displacements

4. Fragility functions

Simplified models of RC wall buildings described in previous sections were used to perform IDA. The inter-story drift of the first story was considered as engineering demand parameter EDP, and it was calculated in terms of a selected intensity measure (IM). In this case, spectral acceleration at the fundamental period of the buildings $Sa(T_1)$ was considered. Finally, the calculated EDP was related to specific damage measure (DM) in order to obtain fragility functions by means of DM versus IM. The probability of exceedance (POE) of each damage state was adjusted to lognormal fragility functions.

4.1 Ground motions

The North-South components of ground motions recorded during the 2010 Chilean earthquake in 14 stations (Table 1) were considered. Fig. 9 shows the individual and mean response spectrum for the 14 components used, and the comparison with the design spectrum of the current code decree N°61 [22]. The definition of the design spectrum considered seismic zone 2 and soil type C. The mean response spectra match the code design spectrum reasonably, with apparent additional energy in the high-frequency range.

Table 1 – Selected ground motions

Station Name	Channel	PGA [g]	Sa($T_{1\ PRE2010}$) [g]	Sa($T_{1\ POST2010}$) [g]
Angol	NS	0.874	0.188	0.297
Curicó	NS	0.469	0.422	0.393
Hualané	NS	0.453	0.496	0.645
Llolleo	NS	0.574	0.525	0.766
Matanzas	NS	0.276	0.390	0.382
Stgo. Centro	NS	0.312	0.236	0.271
Stgo. La Florida	NS	0.186	0.207	0.205
Stgo. Maipú	NS	0.554	0.393	0.549
Stgo. Peñalolén	NS	0.291	0.208	0.233
Stgo. Puente Alto	NS	0.263	0.327	0.333
Talca	NS	0.416	0.365	0.381
Valparaíso Almendral	NS	0.269	0.434	0.575
Viña Centro	NS	0.233	0.439	0.593
Viña El Salto	NS	0.348	0.721	1.033

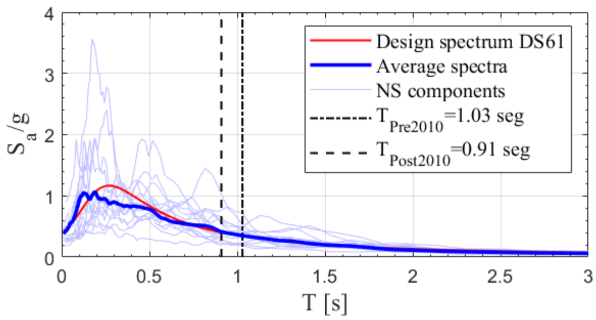

Fig. 9 – Pseudo-acceleration response spectra for selected ground motions considering 5% damping.

4.2 Damage states definition

Damage measures (DM) describe the potential damage state of the structure after an earthquake as a function of the imposed EDP. Damage states proposed by FEMA in HAZUS-HM [9] for RC shear-walls buildings were considered: slight, moderate, extensive, and complete. According to the classification of buildings defined in HAZUS-HM, selected buildings correspond to C2H (High-rise concrete shear walls buildings). Table 2 shows the damage states and moderate-code inter-story drift threshold values considered.

Table 2 – Inter-story drift threshold values [mm/mm] - Moderate-code seismic

Slight	Moderate	Extensive	Complete
0.0020	0.0042	0.0116	0.0300

4.3 Incremental dynamic analysis

Incremental dynamic analysis involves subjecting a structural model to ground motion records, and each scaled to multiple levels of intensity [8]. The ground motions were scaled using the pseudo-acceleration at the fundamental period of each building to obtain a Sa(T_1) value within the range of 0.05g to 1.45g with intensity increments of 0.1g that reflect different levels of IM. In order to relate the EDP obtained of nonlinear analyses with a specific damage state, the maximum inter-story drift of the first story was calculated for each scaled record and compared with the threshold values (Table 2). When each damage state was achieved during the analysis, the corresponding IM value was saved. This process produced a set of IM values associated with the beginning of each damage state for each ground motion, as illustrated in Fig.10a and Fig.10b for the conventional (SFEM-Pre2010) and repaired building (SFEM-Post2010). The green, yellow, orange, and red dots represent the intensity measure at which the slight, moderate, extensive, and complete damage states are achieved, respectively.

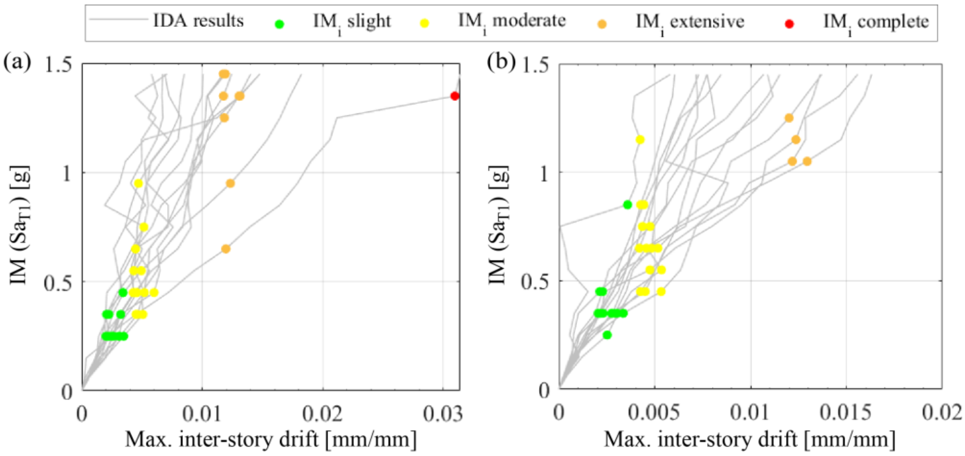

Fig. 10 – IDA curves for peak inter-story drift of the first story: (a) SFEM-Pre2010; (b) SFEM-Post2010

4.4 Fragility analysis results

Since not all levels of damage are achieved for each nonlinear analysis, the truncated IDA procedure described by Baker [24] was used to build the fragility curves. The parameters of the fragility function, i.e., median (θ) and logarithmic standard deviation (β) were obtained using the maximum likelihood method, the values associated with each limit state are shown in Table 3. The Fig.11a corresponds to the fragility curves for the conventional building. The ordinate of response spectra at the fundamental period of the building for the North-South component of the Puente Alto record was $Sa(T_1)$=0.327g. The corresponding POE is 80% and 7% for slight and moderate damage, respectively. The predicted 7% of POE for moderate damage is not found to be reasonable with the real damage observed after the 2010 Chile earthquake, where crushing of concrete and buckling of reinforcement were observed. These physical descriptions of damage in RC walls correspond to those described for extensive damage [9]. Simplified FEM also predicted extensive damage for the North-South component of the Puente Alto record, associated with low drift ratios and high axial loads in the walls. Therefore, the limit states defined in terms of inter-story drift threshold values by FEMA could underestimate the real damage states of this type of buildings. Fig.11b shows the fragility curves for the repaired building. For the North-South component of the Puente Alto record, a $Sa(T_1)$=0.333g was obtained. The POE is 32% and 1% for slight and moderate damage.

The comparison between the fragility curves is shown in Fig.11c. Overall, given a certain IM, the POE of DM is larger for the conventional building. For example, considering the highest ordinate of response spectra at the fundamental period (Table 1), Sa (T_1)=1.033g, the POE of the moderate limited state is 15% and 6.5% for SFEM-Pre2010 and SFEM-Post2010, respectively. The POE of the latter does not decrease significantly. However, this could occur because the limit states defined in terms of inter-story drift threshold values are not adequate for this typology of buildings.

Table 3 – Median and logarithmic standard deviations of the fragility functions

Limit state	**SFEM-Pre2010**		**SFEM-Post2010**	
	θ	**β**	**θ**	**β**
Slight	0.2808	0.1918	0.3773	0.2602
Moderate	0.4928	0.2814	0.6480	0.2635
Extensive	1.4474	0.3273	1.7227	0.3395
Complete	1.7762	0.1400	10.2597	0.1584

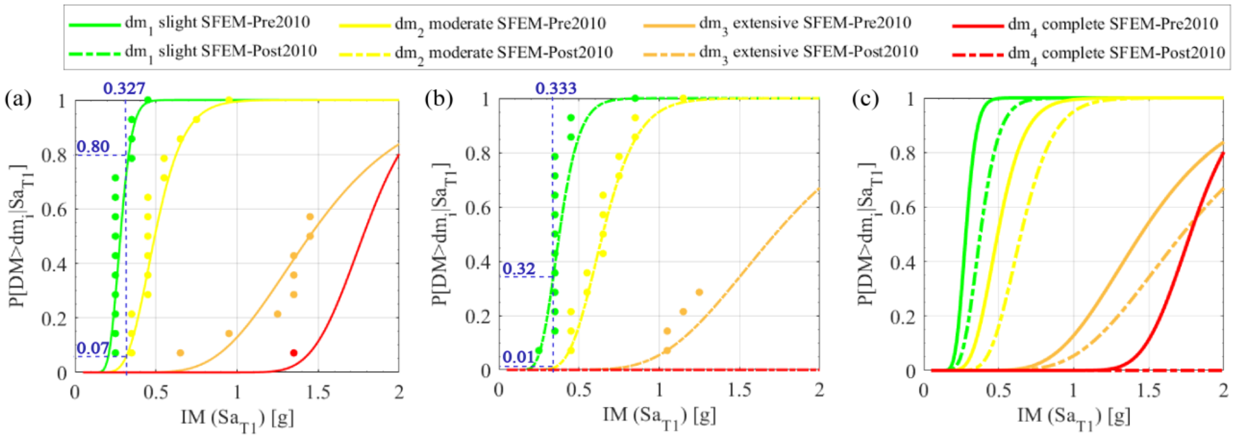

Fig. 11 – Fragility curves: (a) SFEM-Pre2010; (b) SFEM-Post2010; (c) comparison

5. Concluding remarks

This research proposes a simplified analytical FEM that allows for performing IDA within reasonable computational time while capturing the nonlinear structural behavior reliably. A real RC wall building damaged during the 2010 Chile earthquake is considered as a case-study building, and two conditions are evaluated. First, the building is modeled considering its original condition, i.e., thin unconfined walls. Second, the building is evaluated considering its repaired condition, i.e., thicker and confined walls. Fragility curves were built for the two building conditions to compare the behavior of the typical Chilean RC wall buildings constructed before 2010, with the behavior of buildings either repaired after the 2010 earthquake or constructed after 2011 changes in code provisions. For the moderate limit state, the fragility curves show a 7% POE for the building on its original condition, and 1% for the building on its repaired condition, given an IM of Sa(T_1) for the North-South component of the Puente Alto record. The reduction of POE occurred due to the addition of special boundary elements and the increase in the wall thickness. The repaired building complies with the requirements of current seismic design codes. Hence, the changes in code previsions result in a decrease of POE, mainly for extensive and complete damage states. The predicted 7% of POE for moderate damage for the building on its original condition is not found to be reasonable with the extensive damage predicted by the simplified FEM for the same record or with the damage observed after the 2010 Chile earthquake. Chilean RC wall buildings, typically intended for residential use, are stiff due to their large wall density. Therefore, the limit states defined in terms of inter-story drift threshold values by FEMA could underestimate the real damage states of this type of buildings. In order to obtain representative fragility curves in future studies, different performance limits will be proposed, such as the ALR, which was key in the observed damage in Chilean RC wall buildings.

6. Acknowledgements

This research has been funded by the National Science and Technology Council of Chile (CONICYT), CONICYT/FONDECYT/11170514 and the Research Center for Integrated Disaster Risk Management (CIGIDEN), CONICYT/FONDAP/15110017. The first author also acknowledges the support of CONICYT PFCHA/DOCTORADO BECAS CHILE/2018-21181019. The strong motion database used in this work was provided by the project SIBER-RISK, CONICYT/FONDECYT/1170836.

7. References

[1] Mejia LG, Ortiz JC, Osorio LI (2004): RC Structural Wall Buildings. *World Housing Encyclopedia*, Report, 109.

[2] Kam WY, Pampanin S, Elwood K (2011): Seismic performance of reinforced concrete buildings in the 22 February Christchurch (Lyttleton) earthquake. *Bulletin of the New Zealand Society for Earthquake Engineering*, **44**(4), 239-278.

[3] Günay S, Mosalam KM (2013): PEER performance-based earthquake engineering methodology, revisited. *Journal of Earthquake Engineering*, **17**(6), 829-858.

[4] Wallace JW, Massone LM, Bonelli P, Dragovich J, Lagos R, Lüders C, Moehle J (2012): Damage and implications for seismic design of RC structural wall buildings. *Earthquake Spectra*, **28**(S1), S281-S299.

[5] Westenenk B, de la Llera JC, Jünemann R, Hube MA, Besa JJ, Lüders C, Inaudi JA, Riddell R, Jordán R (2013): Analysis and interpretation of the seismic response of RC buildings in Concepción during the February 27, 2010, Chile earthquake. *Bulletin of Earthquake Engineering*, **11**(1), 69-91.

[6] Jünemann R, de la Llera JC, Hube MA, Vásquez JA, Chacón MF (2016): Study of the damage of reinforced concrete shear walls during the 2010 Chile earthquake. *Earthquake Engineering & Structural Dynamics*, **45**(10), 1621-1641.

[7] Calderón JA (2007): Update on structural system characteristics used in RC building construction in Chile. *Civil Engineering Thesis*, University of Chile (in Spanish).

[8] Vamvatsikos D, Cornell CA (2002): Incremental dynamic analysis. *Earthquake Engineering & Structural Dynamics*, **31** (3), 491-514.

[9] Department of Homeland Security, FEMA (2015): HAZUS-MH 2.1. *Earthquake Model Technical Manual*, Washington, D.C., USA.

[10] Jünemann R, de la Llera JC, Hube MA (2017): Analytical methods to assess the collapse and damage of reinforced concrete walls. *Proceedings of the 16th World Conference on Earthquake Engineering*, Santiago, Chile.

[11] DIANA FEA (2017): User's Manual. Delft, Netherlands.

[12] Nakamura H, Higai T (2001): Compressive fracture energy and fracture zone length of concrete. *Modeling of inelastic behavior of RC structures under seismic loads*, 471-487.

[13] Dazio A, Beyer K, Bachmann H (2009): Quasi-static cyclic tests and plastic hinge analysis of RC structural walls. *Engineering Structures*, **31**(7), 1556-1571.

[14] Papadrakakis M, Charmpis DC, Tsompanakis Y, Lagaros ND (2008): *Computational Structural Dynamics and Earthquake Engineering*. Structures and Infrastructures Book Series, 2nd edition.

[15] Mander J, Priestley M, Park R (1988): Theoretical stress-strain model of confined concrete. *Journal of Structural Engineering,* **114**(8), 1804–1826.

[16] Karthik M, Mander J (2011): Stress-block parameters for unconfined and confined concrete based on a unified stress-strain model. *Journal of Structural Engineering*, **137** (2),270-273.

[17] Tagle SJ, Jünemann R, Vásquez JA, de la Llera JC (2019): Double pushover analysis of a RC wall building subjected to earthquake and tsunami in sequence. *Proceedings of the 12th Chilean Conference on Seismology and Earthquake Engineering,* Valdivia, Chile.

[18] Chacón MF, de la Llera JC, Hube MA, Marques J, Lemnitzer A (2017): Epistemic uncertainty in the seismic response of RC free-plan buildings. *Engineering Structures*, 141, 687-702.

[19] Instituto Nacional de Normalización (2008): Reinforced concrete- design and calculation requirements, *NCh430 Of. 2008*. Santiago, Chile (in Spanish).

[20] Instituto Nacional de Normalización (2009). Earthquake resistant design of buildings*, NCh433 Of. 1996 Mod 2009*. Santiago, Chile (in Spanish).

[21] DS N 60 MINVU (2010): Reinforced concrete design code, replacing DS N 118. Chilean Ministry of Housing and Urbanism (in Spanish).

[22] DS N 61 MINVU (2011): Building seismic design code, replacing DS N 117, 2010. Chilean Ministry of Housing and Urbanism (in Spanish).

[23] Hube M, Gálvez H, Jünemann R, Elwood K, Friday J (2018): Repaired Reinforced Concrete Wall Buildings in Chile After 2010 Maule Earthquake. *Proceedings of the 11th National Conference on Earthquake Engineering,* Los Angeles, California, USA.

[24] Baker JW (2015): Efficient analytical fragility function fitting using dynamic structural analysis. *Earthquake Spectra*, **31**(1), 579-599.

